Chemical Science

ROYAL SOCIETY OF CHEMISTRY

EDGE ARTICLE

View Article Online
View Journal | View Issue

Cite this: *Chem. Sci.*, 2023, **14**, 2237

All publication charges for this article have been paid for by the Royal Society of Chemistry

Highly efficient Förster resonance energy transfer between an emissive tetraphenylethylene-based metal–organic cage and the encapsulated dye guest†

Danyang Li,[a] Xin Liu,[a] Linlin Yang,[b] Hechuan Li,[a] Guoxu Guo,[a] Xuezhao Li[a] and Cheng He*[a]

The host–guest strategy presents an ideal way to achieve efficient Förster resonance energy transfer (FRET) by forcing close proximity between an energy donor and acceptor. Herein, by encapsulating the negatively charged acceptor dyes eosin Y (**EY**) or sulforhodamine 101 (**SR101**) in the cationic tetraphenylethene-based emissive cage-like host donor **Zn-1**, host–guest complexes were formed that exhibit highly efficient FRET. The energy transfer efficiency of **Zn-1**⊃**EY** reached 82.4%. To better verify the occurrence of the FRET process and make full use of the harvested energy, **Zn-1**⊃**EY** was successfully used as a photochemical catalyst for the dehalogenation of α-bromoacetophenone. Furthermore, the emission color of the host–guest system **Zn-1**⊃**SR101** could be adjusted to exhibit bright white-light emission with the CIE coordinates (0.32, 0.33). This work details a promising approach to enhance the efficiency of the FRET process by the creation of a host–guest system between the cage-like host and dye acceptor, thus serving as a versatile platform for mimicking natural light-harvesting systems.

Received 1st November 2022
Accepted 30th January 2023

DOI: 10.1039/d2sc06022a

rsc.li/chemical-science

Introduction

Over the past few decades, coordination-driven assembled metal–organic cages have provided a sustainable way to echo the remarkable properties of natural enzymes, due to their facile synthesis, high solubility, and stability in common solvents. With their precisely controlled well-defined cavities, such supramolecular coordination hosts have been widely studied for selective guest encapsulation[1] and recognition,[2] using which highly efficient and stereoselective catalysis has been realized *via* substrate preorganization and the stabilization of reactive intermediates.[3,4] Besides these exciting confinement effects, host–guest systems with their essential components forced close together within the inner space of the cage are also promising candidates to use to develop supramolecular charge/energy donor–acceptor assemblies, which lead to efficient enhancement in energy, electron, or substance transfer, based on short through-space and long through-bond pathways.[5]

Förster resonance energy transfer (FRET) is a classic energy transfer process between different chromophores that proceeds *via* nonradiative dipole–dipole coupling, which has received considerable attention on account of its various applications in photocatalysis,[6] biological imaging,[7] fluorescence probes,[8] and luminescent materials.[9] In addition to matching the spectral overlap between the donor emission and acceptor excitation,[10] effective FRET requires an appropriate distance and dipole orientation between the donor and acceptor.[11] To date, various challenges have been faced using the reported FRET systems linked by covalent bonds (such as porphyrin arrays and dendrimers), such as their time-consuming, multistep synthetic processes, as well as the possibility of emission changes resulting from covalent functionalization.[12] Alternatively, systems formed *via* non-covalent interactions could pave a facile and promising path to construct light-harvesting systems,[13] for example, the chlorophyll–protein system for photosynthesis in green plants.[14]

Inspired by nature, significant advances have been made in mimicking light antenna harvesting systems *via* the FRET process. A wide variety of supramolecular assemblies with noncovalent interactions have been successfully synthesized by designing special scaffolds to accommodate chromophores,[15] such as polymers[16] and organic–inorganic hybrid materials.[17] Challenges in constructing efficient supramolecular FRET systems remain as to how to densely assemble the donor with a high donor–acceptor ratio while avoiding the self-quenching

[a]*State Key Laboratory of Fine Chemicals, Dalian University of Technology, Dalian 116012, P. R. China. E-mail: hecheng@dlut.edu.cn*

[b]*Xinxiang Key Laboratory of Forensic Science Evidence, School of Forensic Medicine, Xinxiang Medical University, Xinxiang 453003, P. R. China*

† Electronic supplementary information (ESI) available: Crystal structures and additional spectroscopic data. CCDC 2195613 and 2195617. For ESI and crystallographic data in CIF or other electronic format see DOI: https://doi.org/10.1039/d2sc06022a

effect induced by molecular aggregation.[18] Therefore, the use of a metal–organic cage as a donor could be a promising approach to assemble light-harvesting systems with highly efficient FRET processes.[6b,c,19] The encapsulation of a guest within the inner cavity of the cage would make the interaction between the donor and the acceptor stronger and more robust in close proximity.[20] Moreover, a highly charged and rigid coordination cage provides an isolated microenvironment in which the donors are fixed and arranged with high local concentration, and decreases the possibility of self-quenching.[21]

Among the building blocks of supramolecular coordination complexes, tetraphenylethene (TPE) has been shown to exhibit unique aggregation-induced emission (AIE) properties, due to the restriction of the rotation of its phenyl ring by coordination bonds, which decreases the nonradiative decay.[22,23] Moreover, quasi C_4-symmetrical TPE-based ligands with multiple phenyl rings are good building blocks to construct face-driven assembled metal–organic cages with confined cavities that can encapsulate suitable guests rigidly. Therefore, TPE-based coordination cages that exhibit good emission would be ideal light-emitting donors for highly efficient energy transfer.

Herein, a highly emissive cage **Zn-1** was constructed as an energy donor *via* face-driven assembly between TPE-based ligands and zinc ions. The cationic cage **Zn-1** is capable of encapsulating negatively charged guests, such as eosin Y (**EY**) or sulforhodamine 101 (**SR101**), as suitable energy acceptors (Scheme 1). It was envisioned that a highly efficient FRET process could be realized between the face-capped host and the dye guests with a high local donor–acceptor ratio and close distance between them. Thus, a systematic investigation of the host–guest chemistry, as well as the FRET process between the donor cage **Zn-1** and acceptor dye **EY** or **SR101**, was conducted. To better verify the occurrence of the FRET process and make full use of the harvested energy, the **Zn-1**⊃**EY** complex was applied as a photochemical catalyst in the dehalogenation of α-bromoacetophenone under ultraviolet (UV) light (365 nm) irradiation, and the **Zn-1**⊃**SR101** complex was shown to function as a white light-emitting system.

Results and discussion

Synthesis and characterization of cage Zn-1

Ligand **L** (L = 4,4′,4″,4‴-(ethene-1,1,2,2-tetrayl)tetrakis(*N*-([2,2′-bipyridin]-5-yl) benzamide)) with four long arms containing bidentate bipyridine units was synthesized by reacting 4,4′,4″,4‴-(ethene-1,1,2,2-tetrayl)tetrabenzoyl chloride with 2,2′-bipyridin-5-amine (Scheme 2). The amide groups were incorporated into the ligand as potential hydrogen bond sites for host–guest binding. Reaction of **L** (6 equiv.) with zinc tetrafluoroborate ($Zn(BF_4)_2$, 8 equiv.) in *N*,*N*-dimethylformamide (DMF) at 80 °C afforded compound **Zn-1** in a yield of 61%. Electrospray ionization mass spectrometry (ESI-MS) measurements on the **Zn-1** solution revealed the formation of a stable

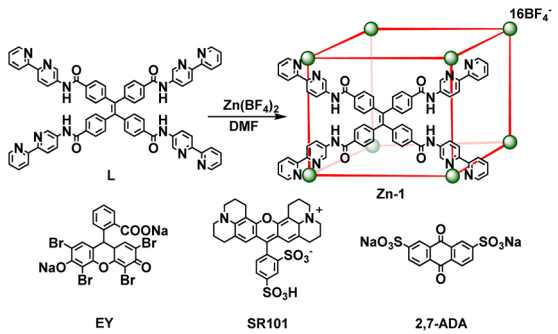

Scheme 2 The self-assembly of cage **Zn-1** and guests **EY**, **SR101**, and 2,7-ADA.

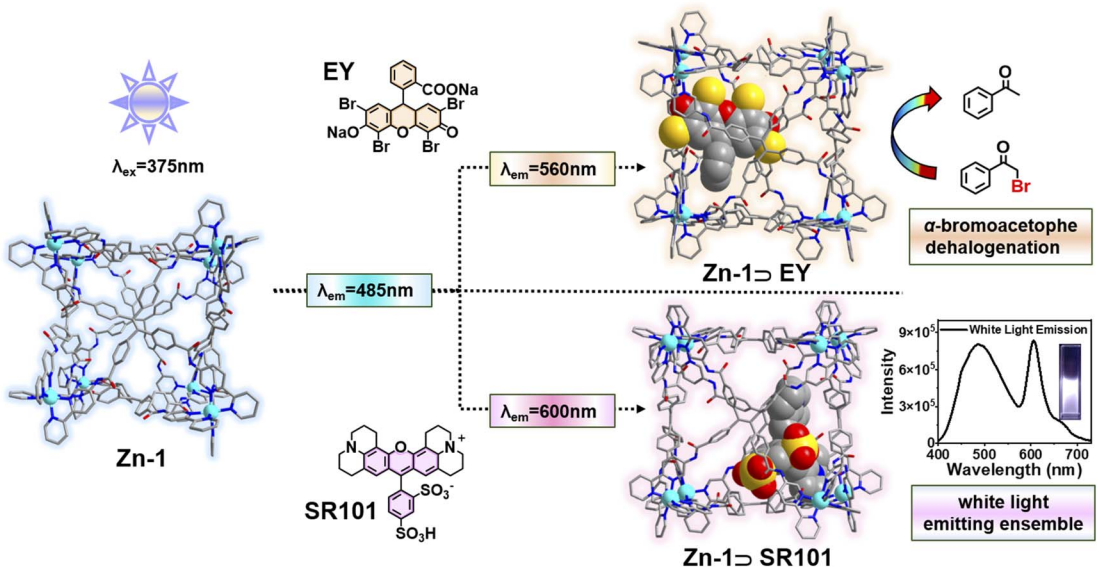

Scheme 1 Illustration of the host–guest strategy between the cage **Zn-1** and the encapsulated negatively charged acceptor dye (**EY** and **SR101**) that induces effective FRET.

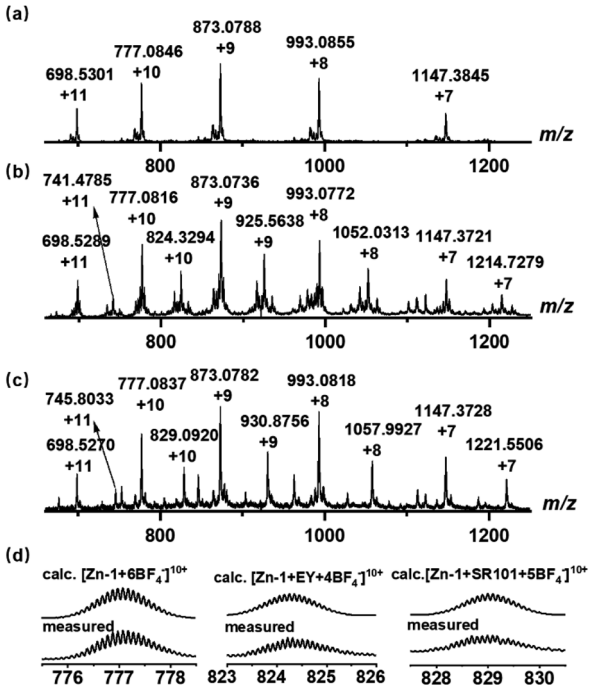

Fig. 1 ESI-MS spectra of the synthesized (a) cage **Zn-1** and host–guest complexes, (b) **Zn-1**⊃**EY**, and (c) **Zn-1**⊃**SR101**. (d) Experimental and calculated peaks.

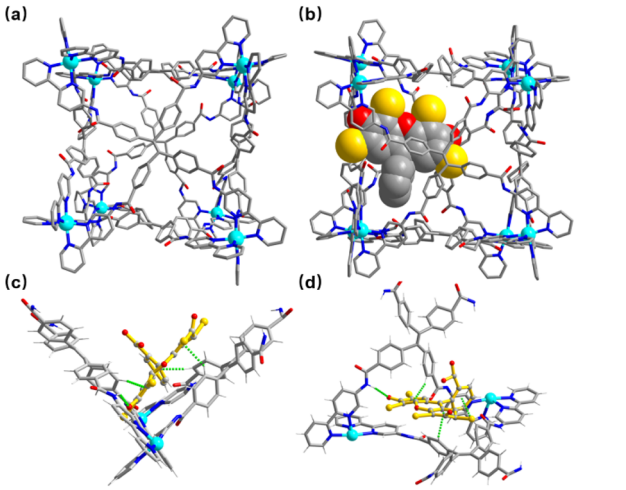

Fig. 2 (a) View of the crystal structure of **Zn-1**; (b) view of the crystal structure of **Zn-1**⊃**EY** (the cavity-bound guest **EY** shows space-filling); (c) and (d) different views showing C–H···π and N–H···O interactions between an **EY** guest and **Zn-1**. Color coding: Zn = cyan; C = gray; N = blue; O = red; Br = yellow. Disorder, anions, and solvent molecules are omitted for clarity.

Zn_8L_6 complex with a characteristic sequence of signals associated with the combination of different numbers of anions that give the target species, which showed isotopically resolved peaks at m/z = 698.5301, 777.0846, 873.0788, 993.0855, and 1147.3845 (Fig. 1a). A simple comparison with the simulation results based on the natural isotopic abundances showed that the resulting peaks could be attributed to $[\mathbf{Zn\text{-}1}\cdot n(BF_4^-)]^{(16-n)+}$ (n = 5–9, with the correct fractional isotope spacings in the high-resolution signals in every case).

A crystal of **Zn-1** suitable for the single-crystal X-ray diffraction study was obtained *via* the slow vapor diffusion of diethyl ether into a DMF/acetonitrile (CH_3CN) solution of **Zn-1** (ESI, Fig. S11a†). The crystal analysis of **Zn-1** confirmed the formation of a face-capped slightly disorder cubic Zn_8L_6 cage with a large cavity (Fig. 2a), where each face of the cage is covered by one TPE-based ligand and each vertex is occupied by an octahedral coordination geometry Zn(II) ion chelated to three 2,2′-bipyridine groups from different TPE-based ligands. The four benzene rings in the TPE moiety are non-coplanar and slightly protrude into the cavity, and the Zn–Zn separations along the cage edges are in the range of 14.86–17.89 Å, giving an inner volume of approximately 4650 Å^3, which could provide a big enough space for large guests, expanding the scope of host–guest chemistry.

The cage **Zn-1** was further characterized by ^{1}H, ^{13}C, and ^{19}F NMR spectroscopies (ESI, Fig. S7–S9†). Most of the ^{1}H NMR signals of **Zn-1** show a slight downfield shift with respect to those of the free ligand **L**. Furthermore, the protons of ligand **L** were split into multiple signals after coordination, indicating the formation of a low-symmetry cage. Additionally, the ^{1}H diffusion-ordered (DOSY) NMR spectrum of **Zn-1** showed the formation of a single species, with a diffusion coefficient (D) value of 3.16 × 10^{-9} m^2 s^{-1} (ESI, Fig. S10†).

Host–guest complexes with encapsulated EY and SR101

The energy acceptors **EY** and **SR101** with suitable absorptions were respectively introduced into the **Zn-1** cage as guests. Electrostatic interactions were expected to be helpful for the binding of the two negatively charged dyes within the positively charged cage. Meanwhile, the planar π-conjugated moiety in **EY** and **SR101** has the potential to form aromatic interactions with the ligand **L** of **Zn-1**. The ESI-MS data of the **Zn-1** solution in the presence of **EY** exhibited a new set of intense peaks at m/z = 741.4785, 824.3294, 925.5638, 1052.0313, and 1214.7279, corresponding to $[\mathbf{Zn\text{-}1}\cdot n(BF_4^-)\cdot\mathbf{EY}]^{(14-n)+}$ (n = 3–7), respectively (Fig. 1b). Moreover, for the solution containing **Zn-1** and **SR101**, new intense peaks appeared at m/z = 745.8033, 829.0920, 930.8756, 1057.9927, and 1221.5506, which were assigned to $[\mathbf{Zn\text{-}1}\cdot n(BF_4^-)\cdot\mathbf{SR101}]^{(15-n)+}$ (n = 4–8), respectively (Fig. 1c). The results thus suggested the possible formation of stable 1 : 1 stoichiometric host–guest complexes in both cases.

The formation of the host–guest complexes was also validated by conducting ^{1}H NMR titration experiments between **Zn-1** and the **EY** or **SR101** guests (Fig. 3a and b, ESI, S13a and b†), and most of the NMR signals of the guests showed slight upfield shifts. Furthermore, H–H interactions between the aromatic rings of **EY** and the aromatic rings of **Zn-1** could be observed in the nuclear Overhauser effect (NOESY) spectrum of **Zn-1**⊃**EY** (ESI, Fig. S15a†), which showed the guest **EY** to reside within the cavity of **Zn-1**. In the NOESY spectrum of **Zn-1**⊃**SR101**, the NOE contacts indicated strong interactions between the protons of the aromatic rings in ligand **L** and the methylene (–CH_2–) protons of **SR101** (ESI, Fig. S15b†). The

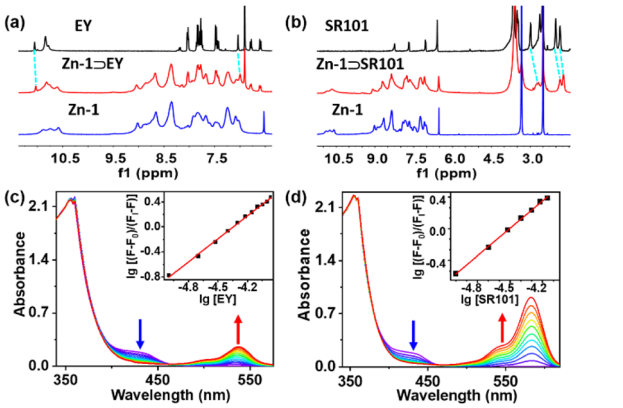

Fig. 3 (a) Sections of the ^{1}H NMR spectra of **Zn-1**, **Zn-1⊃EY**, and **EY** (in DMSO-d_6); (b) sections of the ^{1}H NMR spectra of **Zn-1**, **Zn-1⊃SR101**, and **SR101** (in DMSO-d_6); (c) absorbance spectra of **Zn-1** ([**Zn-1**] = 1.0 × 10^{-5} M) in DMF upon the addition of **EY**. Inset: Hill plot of the titration curve showing the calculation of the associate constant (K = 2.2 × 10^6 M^{-1}); (d) absorbance spectra of **Zn-1** ([**Zn-1**] = 1.0 × 10^{-5} M) in DMF upon the addition of **SR101**. Inset: Hill plot of the titration curve showing the calculation of the associate constant (K = 1.6 × 10^6 M^{-1}).

results thus suggested the presence of potential weak interactions between the ligand and the guests, and indicated that the host and guest were close enough in space for efficient transfer of energy to occur. The binding constants of the guests (**EY** and **SR101**) with **Zn-1** were detected by UV-Vis titration in DMF, using a cooperative 1 : 1 host–guest binding model, with association constants (K) of 2.2 × 10^6 M^{-1} and 1.6 × 10^6 M^{-1} for **EY** and **SR101**, respectively (Fig. 3c and d).

When the guest **EY** or **SR101** was added to a solution of **Zn-1** in DMF in a 4 : 1 ratio and stirred at 80 °C overnight, the faint yellow color of the solution of **Zn-1** turned orange (**Zn-1⊃EY**) or pink (**Zn-1⊃SR101**), respectively. Diffusing diethyl ether into the respective solutions, orange (**Zn-1** with **EY**) or pink (**Zn-1** with **EY**) crystal was obtained (ESI, Fig. S11†). The uniform distribution of **EY** (or **SR101**) in the fluorescence signals of **Zn-1⊃EY** (or **Zn-1⊃SR101**) was investigated by confocal fluorescence microscopy (Fig. 4), where the images suggested that the guest dye was encapsulated in the **Zn-1** cage to form co-crystals rather than being adsorbed on the external surface of the crystals.

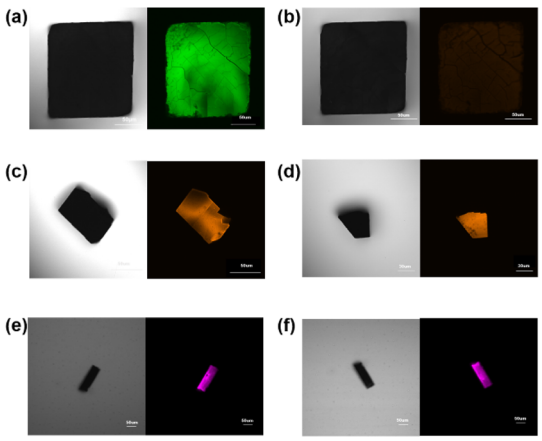

Fig. 4 Confocal images of **Zn-1** (a and b), **Zn-1⊃EY** (c and d), and **Zn-1⊃SR101** (e and f). Bright-field images (left) and dark-field images (right); (a, c and e) detected at λ_{em} = 440–500 nm through a 405 nm filter; (b) detected at λ_{em} = 440–500 nm; (d) detected at λ_{em} = 530–580 nm; (f) detected at λ_{em} = 580–630 nm, through a 488 nm filter.

Although the crystal was low in quality, the crystal of encapsulated **Zn-1⊃EY** was still used in single-crystal X-ray diffraction measurements (Fig. 2b). **Zn-1⊃EY** crystallized in the triclinic space group $P\bar{1}$, with the structure of the cage being maintained by Zn–Zn distances in the range of 15.60–17.87 Å. The eosin Y anion with an average refined occupancy of 25% in the cavity of **Zn-1** (*ca.* 1/4 cages formed the host–guest complexes) was located close to the corner of two adjacent TPE-based ligands to obtain a close distance between the donor host **Zn-1** and acceptor **EY**, falling within the necessary range (generally <10 nm) to allow the FRET process to proceed. Although detailed analysis of the host–guest interactions was difficult due to the poor diffraction data as well as the high disorder of the components, some possible weak interactions could still be determined. The nearest C–H···π distances were found to be in the range of 3.05–3.30 Å between the benzene rings of the TPE-based ligand and the aromatic rings of the **EY** (Fig. 2c and d). Moreover, hydrogen bonding interactions seemed to be present between the N–H of the amine group in the ligand and the oxygen atom of **EY**, with a N···O distance of around 3.10 Å. These multiple weak interactions are helpful in maintaining the stability of the host–guest complex.

However, the weak diffraction intensity limited the crystal structure analysis of **Zn-1⊃SR101**. Therefore, density functional theory (DFT) calculations were conducted to show the possible structure of the host–guest complex. The DFT result suggested that **SR101** is encapsulated inside the cavity of **Zn-1** (ESI, Fig. S12†). In the plausible structure of **Zn-1⊃SR101**, the average Zn–Zn distance is 17.40 Å, falling within the experimental range of 14.86–17.89 Å of **Zn-1**. The anionic **SR101** was suggested to be located at the intersection angle between two adjacent TPE-based ligands, similar to the position of **EY** in the **Zn-1** cavity. The C–H···π distance was shown to be approximately 3.71 Å between the inward pointing protons of the TPE-based ligand and the aromatic ring of the **SR101** guest, and the C–H···O distance was around 3.36 Å between the oxygen atom of the TPE-based ligand and the hydrogen atom of **SR101**.

FRET process of the host–guest complexes

The UV-Vis absorption and emission spectra of ligand **L** and cage **Zn-1** in DMF are shown in Fig. S16 in the ESI.† Compared with the free ligand **L**, the absorption spectrum of **Zn-1** underwent a small red shift (from 320 to 355 nm). The free ligand showed a relatively weak and broad emission at 505 nm and the quantum efficiency fluorescence was 3.09% in DMF (ESI, Fig. S17d, Table S3†). The fluorescence spectra of **Zn-1** showed different emission intensities in different solvent systems (ESI, Fig. S18†). Moreover, the emission of **Zn-1** was dramatically enhanced at blue shift to 485 nm and the quantum efficiency fluorescence of **Zn-1** reached 17.89% in DMF (ESI, Fig. S17a†),

due to the motions of the ligand being restricted by coordination bonds, thus decreasing the nonradiative decay.

The absorption of **EY** overlapped well with the emission of **Zn-1** in DMF (Fig. 5a). The 3D fluorescence spectra of **Zn-1**, **EY**, and **Zn-1⊃EY** showed a series of excitation wavelengths with different intensity emissions in DMF (ESI, Fig. S19†). It was found that the optimized excitation wavelengths of **Zn-1⊃EY** were close to the excitation wavelength of **Zn-1**, indicating the possibility that the energy of **Zn-1** was transferred to the guest **EY**. The FRET process was revealed by fluorescence titration of **EY** into a solution of **Zn-1** (Fig. 5b). With the addition of **EY**, the broad emission peak of **Zn-1** at 485 nm gradually decreased, while a new and sharp emission peak for **Zn-1⊃EY** appeared at 560 nm when excited at 375 nm, accompanied by a change in the color of the fluorescence from blue to yellow under UV light. The CIE chromaticity diagram also confirmed the fluorescence color change from blue to yellow following the titration of **EY** (ESI, Fig. S20a†). Alternatively, addition of **Zn-1** to the solution of **EY** showed that the intensity of **Zn-1** and **EY** gradually increased when excited at 375 nm (ESI, Fig. S21a†).

In addition, the FRET process was further evidenced by the decrease in the fluorescence lifetimes (τ) of the donor **Zn-1** upon adding the acceptor **EY** (ESI, Fig. S22, Table S4†). The decay curve of the **Zn-1** assembly was fitted to double exponential decay, which gave fluorescence lifetimes of $\tau_1 = 1.68$ ns and $\tau_2 = 2.97$ ns. Furthermore, the fluorescence lifetimes of the **Zn-1⊃EY** system decreased to $\tau_1 = 1.28$ ns and $\tau_2 = 2.64$ ns, suggesting that the energy was indeed transferred efficiently from **Zn-1** to the **EY** acceptor. The process of FRET between **Zn-1** and the guest was also studied from the increased fluorescence quantum yield (Φ_F) (ESI, Fig. S17, Table S3†).[19] The Φ_F increased to 21.91% for **Zn-1⊃EY**, which was high compared to that of **Zn-1**(17.89%) alone in DMF.

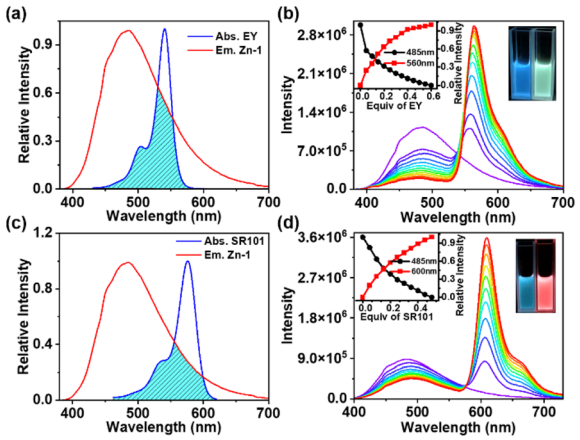

Fig. 5 FRET process between Zn-1 and EY (SR101). (a) Normalized fluorescence spectrum of Zn-1 and absorbance spectrum of EY; (b) fluorescence spectra of Zn-1 ([Zn-1] = 1.0×10^{-5} M) in DMF with different concentrations of EY; (c) normalized fluorescence spectrum of Zn-1 and absorbance spectrum of SR101; (d) fluorescence spectra of Zn-1 ([Zn-1] = 1.0×10^{-5} M) in DMF with different concentrations of SR101.

It should be noted that the energy transfer efficiency (Φ_{ET}) was calculated as 82.4% (ESI, Table S5†) for **Zn-1⊃EY** according to the fluorescence intensity of **Zn-1**, which is quite high among those of reported supramolecular light-harvesting systems.[13,15–19] This strong performance suggests that the cage-encapsulated host–guest complex is an excellent platform for light harvesting *via* the FRET process. The host–guest encapsulation drives the close through-space energy transfer between the donor and acceptor, without changing the luminescence properties arising from the introduction of covalent linking. In this supramolecular system, highly emissive **Zn-1** has a large enough cavity into which the dye **EY** could be loaded to prevent its self-aggregation. Thus, the confined environment of **Zn-1** sets a boundary for the **EY** guest, forcing the formation of a closely bound donor–acceptor pair in an intended ratio.

It has been reported that **EY** can be utilized as a photosensitizer to catalyze the dehalogenation of α-bromoacetophenone in the green light region due to its negligible absorption in the UV region.[24] In this process, the cage host serves as an antenna to transfer energy from the UV radiation to **EY** owing to the strong absorption of **Zn-1** in the UV region. Then, the UV light (365 nm) triggers a photocatalytic reaction. As shown in Table 1, in the presence of **Zn-1⊃EY**, the yield of acetophenone was 83.4% under 530 nm irradiation. A slightly low yield (76.1%) was obtained under 365 nm irradiation, indicating that the dehalogenation reaction not only uses green light but also exploits UV light through the absorption of **Zn-1**, expanding the range of the catalytic light source. A control experiment showed that only **EY** under 365 nm irradiation resulted in slight catalytic activity. A low yield (29.9%) was also obtained for free **Zn-1**. Moreover, almost no catalytic activity was observed in the dark for **Zn-1⊃EY**. These results revealed that light energy harvested by **Zn-1** could be efficiently transferred to **EY** within the cage-encapsulated system (ESI, Fig. S25†).

Energy transfer between **Zn-1** and **SR101** was also investigated by conducting fluorescence titration (Fig. 5c and d), fluorescence quantum yield (ESI, Fig. S17, Table S3†), fluorescence reverse titration (ESI, Fig. S21b†), and fluorescence decay

Table 1 Photocatalytic dehalogenation reaction of α-bromoacetophenone[a]

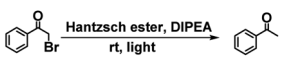

Entry	Source light	Photocatalyst	Yield rate
1	530 nm	**EY**	81.7%
2	530 nm	**Zn-1⊃EY**	83.4%
3	Dark	**Zn-1⊃EY**	n.d.
4	Dark	**EY**	3.1%
5	365 nm	**EY**	n.d.
6	365 nm	**Zn-1⊃EY**	76.1%
7	365 nm	**Zn-1**	29.9%

[a] Reaction conditions: α-bromoacetophenone (20 μmol), Hantzsch ester (22 μmol), DIPEA (7 μl), DMF (1.2 mL), and catalyst (0.5 μmol), Ar, 8 h, rt. All yields were determined by GC analysis.

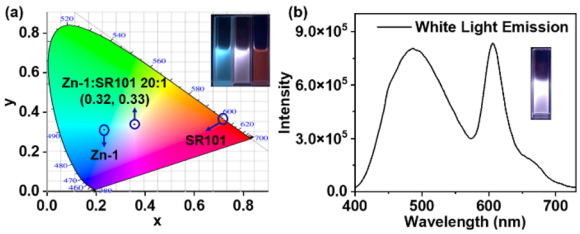

Fig. 6 (a) CIE chromaticity coordinates of **Zn-1**, **SR101**, and **Zn-1⊃SR101**; (b) fluorescence spectrum of the white-light emission coordinate (0.32, 0.33), inset: fluorescence image of the white-light emitting solution, [**Zn-1**] = 1.0×10^{-5} M, [**SR101**] = 5×10^{-7} M.

(Fig. S22, Table S4†) measurements. The Φ_{ET} of **Zn-1⊃SR101** was around 48.8% (ESI, Table S5†). Compared with that of **EY**, the absorption spectrum of **SR101** showed less overlap with the emission of **Zn-1** (Fig. 5c), and as a result, the Φ_{ET} of **Zn-1⊃SR101** was slightly lower.

Encouraged by the emission color area of **Zn-1** (485 nm, cyan color) and **SR101** (600 nm, orange color) which are complementary for white emission, a white-light-emitting material was prepared, a type of material that has attracted much attention in recent years due to its potential uses in illumination and sensing.[25] As expected, strong white-light emission could be attained at a concentration of 1.0×10^{-5} M (**Zn-1**) for a [**Zn-1**]/[**SR101**] molar ratio of 20 : 1 (Fig. 6). The color coordinates of the resulting **Zn-1⊃SR101** system were calculated to be (0.32, 0.33), which are very close to those of a pure white system (0.33, 0.33). Compared with a single-molecule system, host–guest encapsulation is an ideal strategy for constructing a white-light emitting system as the photophysical properties can be easily tuned by altering the non-covalent interactions.

The effect of the host–guest interaction on the FRET processes was also identified by fluorescence titration of **EY** or **SR101** with a solution of ligand **L**. Even though the absorption of **EY** (**SR101**) overlapped well with the emission of **L** in DMF, the broad emission peak of ligand **L** at 505 nm was almost unchanged, with the gradual addition of **EY** (**SR101**) to a solution of ligand **L** (ESI, Fig. S26†).

The FRET process within the cage can be inhibited by binding a competing guest to the enzyme-like host.[26] Anthraquinone-2,7-disulfonic acid disodium salt (2,7-ADA), a negatively charged aromatic anion similar to the dyes **EY** and **SR101**, was employed as a competitive guest and introduced into the host–guest system (ESI, Fig. S27†). With the gradual addition of 2,7-ADA to a solution of **Zn-1⊃EY** (**Zn-1⊃SR101**), the emission peaks of **EY** (**SR101**) and **Zn-1** gradually decreased in intensity (ESI, Fig. S28†), showing that 2,7-ADA acts as an inhibitor, competing with **EY** and **SR101** to be encapsulated in the cage and reducing the FRET process.

Conclusions

In summary, a new emissive TPE-based metal–organic cage **Zn-1** was constructed as an energy donor as well as host to encapsulate the guest acceptors **EY** or **SR101**. The energy acceptors **EY** and **SR101** were matched to generate highly efficient FRET through close space distances forced by the host–guest interactions within the cage. The host–guest complex **Zn-1⊃EY** was shown to serve as a light-harvesting system for the photocatalytic dehalogenation of α-bromoacetophenone. Furthermore, by adjusting the molar ratio of **Zn-1** and **SR101**, bright white-light emission was achieved with the CIE coordinate (0.32, 0.33). Overall, this work was devoted to developing an ideal approach for the creation of a host–guest system *via* cage encapsulation to enhance the efficiency of the FRET process, serving as a versatile platform for mimicking natural light-harvesting systems.

Experimental

Preparation of Zn-1

A mixture of **L** (101 mg, 0.09 mmol) and zinc tetrafluoroborate (28.6 mg, 0.12 mmol) was dissolved in 30 mL DMF. The resulting reaction mixture was then heated at 80 °C for 12 hours. This solution was thereafter added to diethyl ether and the product was obtained after centrifugation and drying. The desired product was obtained as a light brown solid in 61% yield (based on the solid dried under vacuum). ^{1}H NMR (400 MHz, DMSO-d_6): δ = 10.77 (s, 1H), 9.04–8.65 (m, 3H), 8.52–8.00 (m, 3H), 7.77–7.48 (m, 3H), 7.05 (dd, J = 23.4, 15.3 Hz, 2H). ^{13}C NMR (101 MHz, DMSO-d_6): δ = 166.69, 148.50, 147.54, 146.16, 145.51, 143.54, 142.02, 139.83, 139.30, 139.01, 136.85, 132.74, 130.78, 127.77, 127.64, 127.20, 123.94, 122.92. ^{19}F NMR (400 MHz, DMSO-d_6): δ = −148.22.

General procedure for the cage-based catalysis

DMF (1.2 ml), α-bromoacetophenone (4.0 mg, 0.02 mmol), diethyl-2,6-dimethyl-1,4-dihydropyridine-3,5-dicarboxylate (Hantzsch ester) (5.6 mg, 2.2×10^{-2} mmol), *N*,*N*-diisopropylethylamine (DIPEA) (7.0 μl, 0.07 mmol), and catalyst (**Zn-1** 4.32 mg, 5×10^{-4} mmol and **EY** 0.35 mg, 5×10^{-4} mmol) were added to a 5 mL flask. The flask was sealed with a septum, and then degassed by bubbling with argon gas for 15 min under atmospheric pressure at room temperature. After that, the mixture was irradiated using a light source at room temperature for 8 h. The product was monitored by gas chromatography relative to the internal standard 1,3,5-trimethoxybenzene.

Crystallography

Crystals of **Zn-1** and the host–guest complex **Zn-1⊃EY** suitable for X-ray diffraction measurements were obtained *via* the slow diffusion of diethyl ether into a mixed DMF and CH_3CN solution of the complex over a few days. The acquired crystals were found to be hypersensitive to the loss of solvent. In spite of rapid handling times and low-temperature data collection, the quality of the data was less than ideal.

Crystal data of **Zn-1**: $C_{422}H_{299}B_{11.50}F_{47}N_{72}O_{27.75}Zn_8$, M = 8362.59, monoclinic, space group $P2_1/c$, white block, a = 27.515(2), b = 48.566(3), c = 55.058(3) Å, β = 91.649(1), V = 73 544(7) Å^3, Z = 4, D_c = 0.755 g cm^{-3}, μ(MoKα) = 0.309 mm^{-1}, T =

120(2) K. 129 439 unique reflections [R_{int} = 0.1120]. Final R_1 [with $I > 2\sigma(I)$] = 0.1153, wR_2 (all data) = 0.3155 for the data collected. CCDC number 2195613.†

Crystal data of **Zn-1⊃EY:** $C_{453.50}H_{351.50}B_{7.50}BrF_{30}N_{77.50}O_{62}Zn_8$, M = 9132.55, triclinic, space group $P\bar{1}$, orange block, a = 27.217(7), b = 33.119(7), c = 38.817(2) Å, α = 88.598(2), β = 88.357(1), γ = 83.075(2), V = 34 712(3) Å^3, Z = 2, D_c = 0.874 g cm^{-3}, μ(Mo-Kα) = 0.71073 mm^{-1}, T = 180(2) K. 122 093 unique reflections [R_{int} = 0.1005]. Final R_1 [with $I > 2\sigma(I)$] = 0.1497, wR_2 (all data) = 0.450 for the data collected. CCDC number 2195617.†

Data availability

All the data supporting this article have been included in the main text and the ESI.†

Author contributions

C. He and D. Li designed the research and co-wrote the manuscript. D. Li, H. Li, and G. Guo performed all experiments. X. Liu carried out DFT calculation. L. Yang and X. Li assisted in analyzing the data.

Conflicts of interest

There are no conflicts to declare.

Acknowledgements

This work was supported by the National Natural Science Foundation of China (22171033, 21701019, and 21573034) and the Fundamental Research Funds for the Central Universities [DUT17RC(3)094].

Notes and references

1 (*a*) T. R. Cook and P. J. Stang, *Chem. Rev.*, 2015, **115**, 7001–7045; (*b*) R. Chakrabarty, P. S. Mukherjee and P. J. Stang, *Chem. Rev.*, 2011, **111**, 6810–6918; (*c*) D. Zhang, T. K. Ronson, Y.-Q. Zou and J. R. Nitschke, *Nat. Rev. Chem.*, 2021, **5**, 168–182; (*d*) D. Zhang, T. K. Ronson and J. R. Nitschke, *Acc. Chem. Res.*, 2018, **51**, 2423–2436; (*e*) M. D. Ward, C. A. Hunter and N. H. Williams, *Acc. Chem. Res.*, 2018, **51**, 2073–2082; (*f*) Y. Tamura, H. Takezawa and M. Fujita, *J. Am. Chem. Soc.*, 2020, **142**, 5504–5508.

2 (*a*) M. D. Ludden, C. G. P. Taylor and M. D. Ward, *Chem. Sci.*, 2021, **12**, 12640–12650; (*b*) T. R. Schulte, J. J. Holstein and G. H. Clever, *Angew. Chem., Int. Ed.*, 2019, **58**, 5562–5566; (*c*) X. Jing, C. He, L. Zhao and C. Duan, *Acc. Chem. Res.*, 2019, **52**, 100–109; (*d*) M. Ueda, N. Kishida, L. Catti and M. Yoshizawa, *Chem. Sci.*, 2022, **13**, 8642–8648.

3 (*a*) C. J. Brown, F. D. Toste, R. G. Bergman and K. N. Raymond, *Chem. Rev.*, 2015, **115**, 3012–3035; (*b*) W. Cullen, M. C. Misuraca, C. A. Hunter, N. H. Williams and M. D. Ward, *Nat. Chem.*, 2016, **8**, 231–236; (*c*) R. Saha, B. Mondal and P. S. Mukherjee, *Chem. Rev.*, 2022, **122**, 12244–12307; (*d*) Y. Fang, J. A. Powell, E. Li, Q. Wang, Z. Perry, A. Kirchon, X. Yang, Z. Xiao, C. Zhu, L. Zhang, F. Huang and H.-C. Zhou, *Chem. Soc. Rev.*, 2019, **48**, 4707–4730; (*e*) W.-X. Gao, H.-N. Zhang and G.-X. Jin, *Coord. Chem. Rev.*, 2019, **386**, 69–84; (*f*) L.-X. Cai, S.-C. Li, D.-N. Yan, L.-P. Zhou, F. Guo and Q.-F. Sun, *J. Am. Chem. Soc.*, 2018, **140**, 4869–4876; (*g*) X.-X. Gou, T. Liu, Y.-Y. Wang and Y.-F. Han, *Angew. Chem., Int. Ed.*, 2020, **59**, 16683–16689; (*h*) L. R. Holloway, P. M. Bogie, Y. Lyon, C. Ngai, T. F. Miller, R. R. Julian and R. J. Hooley, *J. Am. Chem. Soc.*, 2018, **140**, 8078–8081; (*i*) V. MartÍ-Centelles, A. L. Lawrence and P. J. Lusby, *J. Am. Chem. Soc.*, 2018, **140**, 2862–2868.

4 (*a*) H. Takezawa, K. Shitozawa and M. Fujita, *Nat. Chem.*, 2020, **12**, 574–578; (*b*) J. Dong, Y. Liu and Y. Cui, *Acc. Chem. Res.*, 2021, **54**, 194–206; (*c*) J.-S. Wang, K. Wu, C. Yin, K. Li, Y. Huang, J. Ruan, X. Feng, P. Hu and C.-Y. Su, *Nat. Commun.*, 2020, **11**, 4675; (*d*) Q.-Q. Wang, S. Gonell, S. H. A. M. Leenders, M. Duerr, I. Ivanovic-Burmazovic and J. N. H. Reek, *Nat. Chem.*, 2016, **8**, 225–230.

5 (*a*) L. Zhao, X. Jing, X.-Z. Li, X.-Y. Guo, L. Zeng, C. He and C.-Y. Duan, *Coord. Chem. Rev.*, 2019, **378**, 151–187; (*b*) M. R. Wasielewski, *Acc. Chem. Res.*, 2009, **42**, 1910–1921; (*c*) W. Cullen, H. Takezawa and M. Fujita, *Angew. Chem., Int. Ed.*, 2019, **58**, 9171–9173; (*d*) H. Sunohara, K. Koyamada, H. Takezawa and M. Fujita, *Chem. Commun.*, 2021, **57**, 9300–9930; (*e*) D. M. Daiton, S. R. Ellis, E. M. Nichols, R. A. Mathies, F. D. Toste, R. G. Bergman and K. N. Raymond, *J. Am. Chem. Soc.*, 2015, **137**, 10128–10131; (*f*) A. J. Musser, P. P. Neelakandan, J. M. Richter, H. Mori, R. H. Friend and J. R. Nitschke, *J. Am. Chem. Soc.*, 2017, **139**, 12050–12059.

6 (*a*) M. Hao, G. Sun, M. Zuo, Z. Xu, Y. Chen, X. Y. Hu and L. Wang, *Angew. Chem., Int. Ed.*, 2020, **59**, 10095–10100; (*b*) D. Zhang, W. Yu, S. Li, Y. Xia, X. Li, Y. Li and T. Yi, *J. Am. Chem. Soc.*, 2021, **143**, 1313–1317; (*c*) Z. Zhang, Z. Zhao, Y. Hou, H. Wang, X. Li, G. He and M. Zhang, *Angew. Chem., Int. Ed.*, 2019, **58**, 8862–8866.

7 (*a*) X.-M. Chen, Q. Cao, H. K. Bisoyi, M. Wang, H. Yang and Q. Li, *Angew. Chem., Int. Ed.*, 2020, **59**, 10493–10497; (*b*) X.-F. Hou, S. Zhang, X. Chen, H. K. Bisoyi, T. Xu, J. Liu, D. Chen, X.-M. Chen and Q. Li, *ACS Appl. Mater. Interfaces*, 2022, **14**, 22443–22453.

8 (*a*) N. Melnychuk, S. Egloff, A. Runser, A. Reisch and A. S. Klymchenko, *Angew. Chem., Int. Ed.*, 2020, **59**, 6811–6818; (*b*) T. Xiao, C. Bao, L. Zhang, K. Diao, D. Ren, C. Wei, Z.-Y. Li and X.-Q. Sun, *J. Mater. Chem. A*, 2022, **10**, 8528–8534.

9 (*a*) Y.-X. Yuan, J.-H. Jia, Y.-P. Song, F.-Y. Ye, Y.-S. Zheng and S.-Q. Zang, *J. Am. Chem. Soc.*, 2022, **144**, 5389–5399; (*b*) H. Liu, Z. Zhang, C. Mu, L. Ma, H. Yuan, S. Ling, H. Wang, X. Li and M. Zhang, *Angew. Chem., Int. Ed.*, 2022, **61**, e202207289.

10 Y. Jiang and J. McNeill, *Chem. Rev.*, 2017, **117**, 838–859.

11 (*a*) K. Wang, K. Velmurugan, B. Li and X.-Y. Hu, *Chem. Commun.*, 2021, **57**, 13641–13654; (*b*) J.-J. Li, H.-Y. Zhang, X.-Y. Dai, Z.-X. Liu and Y. Liu, *Chem. Commun.*, 2020, **56**, 5949–5952; (*c*) K. Diao, D. J. Whitaker, Z. Huang, H. Qian,

D. Ren, L. Zhang, Z.-Y. Li, X.-Q. Sun, T. Xiao and L. Wang, *Chem. Commun.*, 2022, **58**, 2343–2346.

12 (*a*) J. Yang, M.-C. Yoon, H. Yoo, P. Kim and D. Kim, *Chem. Soc. Rev.*, 2012, **41**, 4808–4826; (*b*) Y.-H. Jeong, M. Son, H. Yoon, P. Kim, D.-H. Lee, D. Kim and W.-D. Jang, *Angew. Chem., Int. Ed.*, 2014, **53**, 6925–6928; (*c*) P. Parkinson, C. E. I. Knappke, N. Kamonsutthipaijit, K. Sirithip, J. D. Matichak, H. L. Anderson and L. M. Herz, *J. Am. Chem. Soc.*, 2014, **136**, 8217–8220.

13 (*a*) Y.-X. Hu, W.-J. Li, P.-P. Jia, X.-Q. Wang, L. Xu and H.-B. Yang, *Adv. Opt. Mater.*, 2020, **8**, 2000265; (*b*) Q. Song, S. Goia, J. Yang, S. C. L. Hall, M. Staniforth, V. G. Stavros and S. Perrier, *J. Am. Chem. Soc.*, 2021, **143**, 382–389; (*c*) T. Xiao, L. Zhang, H. Wu, H. Qian, D. Ren, Z.-Y. Li and X. Sun, *Chem. Commun.*, 2021, **57**, 5782–5785.

14 A. Melis, *Energy Environ. Sci.*, 2012, **5**, 5531–5539.

15 (*a*) K. Acharyya, S. Bhattacharyya, H. Sepehrpour, S. Chakraborty, S. Lu, B. Shi, X. Li, P. S. Mukherjee and P. J. Stang, *J. Am. Chem. Soc.*, 2019, **141**, 14565–14569; (*b*) Y. Li, S. S. Rajasree, G. Y. Lee, J. Yu, J.-H. Tang, R. Ni, G. Li, K. N. Houk, P. Deria and P. J. Stang, *J. Am. Chem. Soc.*, 2021, **143**, 2908–2919; (*c*) Y. Li, Y. Dong, L. Cheng, C. Qin, H. Nian, H. Zhang, Y. Yu and L. Cao, *J. Am. Chem. Soc.*, 2019, **141**, 8412–8415; (*d*) W.-J. Li, X.-Q. Wang, D.-Y. Zhang, Y.-X. Hu, W.-T. Xu, L. Xu, W. Wang and H.-B. Yang, *Angew. Chem., Int. Ed.*, 2021, **60**, 18761–18768.

16 (*a*) Y.-N. Jing, S.-S. Li, M. Su, H. Bao and W.-M. Wan, *J. Am. Chem. Soc.*, 2019, **141**, 16839–16848; (*b*) L. Xu, Z. Wang, R. Wang, L. Wang, X. He, H. Jiang, H. Tang, D. Cao and B. Z. Tang, *Angew. Chem., Int. Ed.*, 2020, **59**, 9908–9913.

17 (*a*) M. Zeng, A. Ren, W. Wu, Y. Zhao, C. Zhan and J. Yao, *Chem. Sci.*, 2020, **11**, 9154–9161; (*b*) Q. Mu, J. Liu, W. Chen, X. Song, X. Liu, X. Zhang, Z. Chang and L. Chen, *Chem.–Eur. J.*, 2019, **25**, 1901–1905.

18 C. Li, J. Zhang, S. Zhang and Y. Zhao, *Angew. Chem., Int. Ed.*, 2019, **58**, 1643–1647.

19 (*a*) K. Acharyya, S. Bhattacharyya, S. Lu, Y. Sun, P. S. Mukherjee and P. J. Stang, *Angew. Chem., Int. Ed.*, 2022, **61**, e202200715; (*b*) J. R. Piper, L. Cletheroe, C. G. P. Taylor, A. J. Metherell, J. A. Weinstein, I. V. Sazanovich and M. D. Ward, *Chem. Commun.*, 2017, **53**, 408.

20 D. R. Martir, A. Pizzolante, D. Escudero, D. Jacquemin, S. L. Warriner and E. Zysman-Colman, *ACS Appl. Energy Mater.*, 2018, **1**, 2971–2978.

21 A. Kumar, R. Saha and P. S. Mukherjee, *Chem. Sci.*, 2021, **12**, 5319–5329.

22 (*a*) J. Mei, N. L. C. Leung, R. T. K. Kwok, J. W. Y. Lam and B. Z. Tang, *Chem. Rev.*, 2015, **115**, 11718–11940; (*b*) Y. Hong, J. W. Y. Lam and B. Z. Tang, *Chem. Soc. Rev.*, 2011, **40**, 5361–5388.

23 (*a*) X. Yan, T. R. Cook, P. Wang, F. Huang and P. J. Stang, *Nat. Chem.*, 2015, **7**, 342–348; (*b*) Z. Guo, G. Li, H. Wang, J. Zhao, Y. Liu, H. Tan, X. Li, P. J. Stang and X. Yan, *J. Am. Chem. Soc.*, 2021, **143**, 9215–9221; (*c*) X. Yan, M. Wang, T. R. Cook, M. Zhang, M. L. Saha, Z. Zhou, X. Li, F. Huang and P. J. Stang, *J. Am. Chem. Soc.*, 2016, **138**, 4580–4588; (*d*) V. M. Suresh, A. De and T. K. Maji, *Chem. Commun.*, 2015, **51**, 14678–14681; (*e*) P. Sutar, V. M. Suresh, K. Jayaramulu, A. Hazra and T. K. Maji, *Nat. Commun.*, 2018, **9**, 3587–3598.

24 M. Neumann, S. Füldner, B. König and K. Zeitler, *Angew. Chem., Int. Ed.*, 2011, **50**, 951–954.

25 (*a*) H.-T. Feng, X. Zheng, X. Gu, M. Chen, J. W. Y. Lam, X. Huang and B. Z. Tang, *Chem. Mater.*, 2018, **30**, 1285–1290; (*b*) Q. Song, S. Goia, J. Yang, S. C. L. Hall, M. Staniforth, V. G. Stavros and S. Perrier, *J. Am. Chem. Soc.*, 2021, **143**, 382–389.

26 J. Wei, L. Zhao, C. He, S. Zheng, J. N. H. Reek and C. Duan, *J. Am. Chem. Soc.*, 2019, **141**, 12707–12716.